Spontaneous Emission and Resonant Scattering in Transition from Type I to Type II Photonic Weyl Systems

Yang Yang,[1,2,*] Wenlong Gao,[2,*] Lingbo Xia,[2] Hua Cheng,[2] Hongwei Jia,[1,2]
Yuanjiang Xiang,[1,†] and Shuang Zhang[2,‡]

[1]*Key Laboratory of Optoelectronic Devices and Systems of Ministry of Education and Guangdong Province, College of Optoelectronic Engineering, Shenzhen University, Shenzhen 518060, China*

[2]*School of Physics and Astronomy, University of Birmingham, Birmingham B15 2TT, United Kingdom*

(Received 21 December 2018; published 15 July 2019)

Spontaneous emission and scattering behavior of an emitter or a resonant scatterer strongly depend on the density of states of the surrounding medium. It has been shown that the resonant scattering cross section (RSC) may diverge at the Weyl frequency of a type I Weyl system due to the diminishing density of states. Here we study the spontaneous emission (SE) and RSC in a photonic metacrystal across the critical transition between type I and type II Weyl systems. Theoretical results show that the SE rate of an emitter in a type I Weyl system diminishes to zero at the Weyl frequency. When the system is tuned towards the transition point between type I and type II Weyl point, the dip in the SE spectrum at the Weyl frequency becomes infinitely sharp. The dip vanishes at the critical transition, and transforms into a peak when the system changes into a type II Weyl system. We further show that the resonant scattering cross section also exhibits dramatically different spectral features across the transition. Our study demonstrates the ability to tune SE and RSC through altering the dispersion of the Weyl medium between type I and type II, which provides a fundamentally new route in manipulating light-matter interactions.

DOI: 10.1103/PhysRevLett.123.033901

Spontaneous emission (SE) is of great importance to many applications from light-emitting devices to biological and medical imaging. The rate of SE is determined by the electromagnetic interaction between an atom and a quantum field, which can be tuned by varying the electromagnetic environment of the source [1,2]. Modification of SE in photonic environments can be implemented in photonic crystals [3–6], nanoscale cavities [7,8], plasmonic nanostructures [9,10], and metamaterials [11,12]. In an atomic system, the rate of SE is closely related to its cross section of resonant scattering, as both are strongly dependent on the density of states (DOS) of the optical environment.

Topological phases such as topological insulators and topological semimetals have been extensively studied in condensed matter physics because they support edge states or surface states that are immune from scattering [13,14]. These novel concepts have been recently extended to classical systems such as photonics and acoustics [15,16]. In photonics, photonic structures such as photonic crystals [17,18] and metamaterials [19] that support nontrivial topological surface states have been studied both in theory and experiment. Besides photonic analogs of topological insulators, three dimensional photonic crystals and metamaterials that support Weyl points have been proposed and realized [20–24]. Weyl points are linear crossings between two bands at isolated points in the three dimensional momentum space or synthetic space. They can be viewed as monopoles of quantized monopole charge in the momentum space, acting as sources or drains of the Berry curvature, with the sign of the monopole charge determined by the Weyl point's chirality. Depending on the DOS at the Weyl frequencies, Weyl systems can be categorized as type I with a diminishing DOS and type II with a finite DOS [25,26]. Because of this dramatic difference, it is expected that DOS related phenomena such as SE and resonant scattering exhibit very different behaviors in these two types of photonic Weyl systems. In this work, we design a realistic Weyl metamaterial whose Weyl degeneracies can be continuously tuned from type I to type II across the critical transition and investigate the behavior of SE and the resonant scattering cross section (RSC) across this transition. It is found that the SE spectrum transits from a dip in type I into a peak in type II, while the diverging RSC in a type I Weyl system turns into a minimum at the Weyl frequency in a type II system. Across the transition between type I and type II, extremely sharp spectral features are present for the SE, which may be employed for sensing applications.

We start by considering an ideal Weyl system consisting of a number of Weyl points located at exactly the same frequency, which are related to each other through symmetry operations [27]. Using the two degenerate modes at the Weyl points as the basis, the general effective Hamiltonian close to each Weyl point can be expressed as

$$H_{\text{eff}} = N_x k_x \sigma_x + N_y k_y \sigma_y + N_z k_z \sigma_z + T_x k_x I, \quad (1)$$

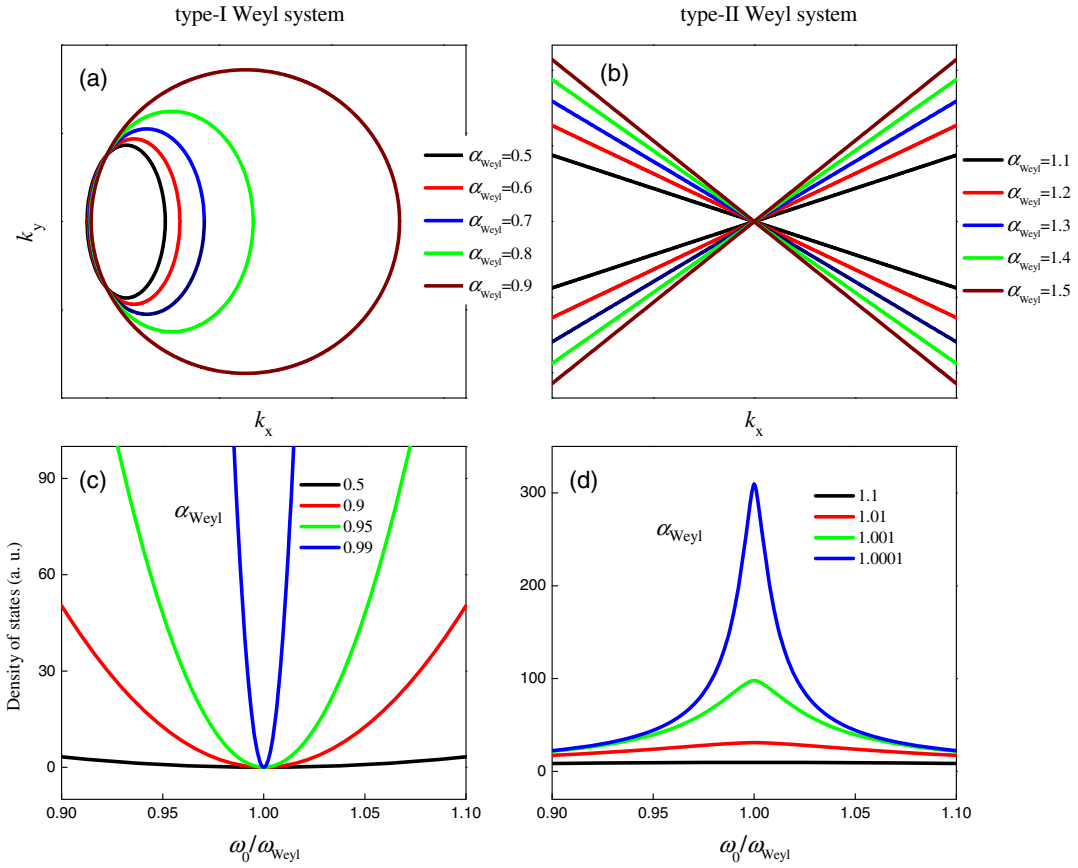

FIG. 1. Transformation of the isofrequency surface of a type I (a) and type II (b) Weyl point according to a different Weyl parameter α_{Weyl} in the k_x-k_y plane. (c) and (d) The transformation of density of states in type I and type II Weyl systems with different α_{Weyl}, respectively.

where $\sigma_{x,y,z}$ are Pauli matrices, I is a 2×2 identity matrix, $N_{x,y,z}$ are the Fermi velocities, and T_x is the tilted velocity of the Weyl point along the x direction. The tilting of the Weyl dispersion cone is determined by the Weyl parameter $\alpha_{\mathrm{Weyl}} = T_x/N_x$, with $\alpha_{\mathrm{Weyl}} < 1$ corresponding to a type I Weyl system, and $\alpha_{\mathrm{Weyl}} > 1$ corresponding to a type II Weyl system [28]. Both types of Weyl points are topologically nontrivial, but they possess a different DOS, which is expressed as $\mathrm{DOS}_{\mathrm{Weyl}} \propto \iint 1/|\mathbf{v}_{\mathbf{k}}| d^2\mathbf{k}$ [29–31]. The DOS is directly related to the area of isofrequency surface. Figure 1 shows the transformation of the isofrequency surface for different Weyl parameters α_{Weyl} with (a) $\alpha_{\mathrm{Weyl}} = 0.5$–$0.9$, corresponding to a type I Weyl point with frequency fixed as $\omega = 0.9\omega_{\mathrm{Weyl}}$, and (b) $\alpha_{\mathrm{Weyl}} = 1.1$–$1.5$, corresponding to a type II Weyl point with frequency $\omega = \omega_{\mathrm{Weyl}}$, respectively. For simplicity, only the interception of the isofrequency surface with the k_x-k_y plane is plotted, while the 3D isofrequency surface can be visualized by rotating this 2D plot along the k_x axis. As shown in Fig. 1(a), the isofrequency surface of the wave vector is elliptical for the type I Weyl point, and it gradually expands when α_{Weyl} approaches unity, which corresponds to the critical transition. The length of axis of the elliptical isofrequency surface along the k_x, k_y, and k_x direction is expressed as $\tilde{\omega}/[N_x(1-\alpha_{\mathrm{Weyl}}^2)]$, $\tilde{\omega}/[N_y(1-\alpha_{\mathrm{Weyl}}^2)^{1/2}]$, and $\tilde{\omega}/[N_z(1-\alpha_{\mathrm{Weyl}}^2)^{1/2}]$, respectively, where $\tilde{\omega} = \omega_0 - \omega_{\mathrm{Weyl}}$. When approaching the critical transition of the Weyl point, the k_x axis increases much faster than k_y and k_z, leading to an extremely elongated elliptical isofrequency surface. For the type II Weyl point shown in Fig. 1(b), the isofrequency surface turns into two cones with a point contact at the Weyl frequency, the opening angle θ_{open} of the hyperbolic isofrequency cones increases with α_{Weyl} increasing, which follows the relation of $\theta_{\mathrm{open}} = 2\tan^{-1}[(\alpha_{\mathrm{Weyl}}^2-1)^{1/2}N_x/N_y]$.

The corresponding DOS for a type I and type II Weyl medium is shown in Figs. 1(c) and 1(d), respectively. Transformation of DOS of a type I Weyl system can be expressed as $\mathrm{DOS}_{\mathrm{Weyl}} \propto 4\pi\tilde{\omega}^2/[N_xN_yN_z(1-\alpha_{\mathrm{Weyl}}^2)^2]$ (see Sec. I in Ref. [32]). The analytical form shows the DOS in a type I Weyl system ($N_x > T_x$) diminishes when approaching the Weyl frequency. When α_{Weyl} increases towards unity, i.e., approaching the critical transition of the Weyl point, the width of valley in the spectrum of DOS is dramatically reduced, while its minimum remains zero at the Weyl frequency, resulting in extremely sharp spectral

feature in Fig. 1(c). The characteristics of DOS spectra in type I Weyl system can be understood based on the isofrequency surface of Weyl points, which has an elliptical shape. When approaching the Weyl frequency, the ellipsoid shrinks and becomes a point at the Weyl frequency, and consequently the DOS (also the local DOS) decreases to zero, which would result in a diminishing SE.

In the calculation of DOS in type II Weyl system, we impose a two dimensional truncation in the momentum space that is perpendicular to the axis of hyperbolic isofrequency surface with $\mathbf{k}_t = \omega_{\mathrm{Weyl}}/c$ away from the Weyl point to constrain it from divergence, where c is the speed of light in vacuum. This truncation can be understood as a consequence of the finite size of the Brillouin zone in any realistic systems. The isofrequency surface of both type I and type II Weyl system becomes extremely narrow close to the transition point. Interestingly, for a type II Weyl system, the DOS spectra show the opposite trend as that of the type I system. As shown in Fig. 1(d), when approaching the Weyl frequency, the DOS is enhanced and forms a peak. With decreasing α_{Weyl} in type II Weyl regime, the Lorentz peak at the Weyl frequency becomes stronger. The extremely enhanced DOS indicates an enhanced SE in type II Weyl system at the Weyl frequency close to the critical transition, which may be exploited for laser applications.

Next we consider a two-level atom embedded inside the Weyl system, which emits light into the Bloch modes of the Weyl structure. The atom can be considered as a dipole of oscillation frequency ω_0. In the weak coupling regime, the radiating power P is given by the summation over emissions into all the Bloch modes with different wave vector $\mathbf{k}$ across the isofrequency surface [33,39,40]

$$P = \frac{\pi\omega_0^2}{4\varepsilon_0} \iint \frac{|\mathbf{d}\cdot\mathbf{u}_{\mathbf{k}}(\mathbf{r}_0)|^2}{|\mathbf{v}_{\mathbf{k}}|} d^2\mathbf{k}, \tag{2}$$

where $\mathbf{v}_{\mathbf{k}} = \nabla_{\mathbf{k}}\omega_{\mathbf{k}}$ is the group velocity of the eigenwave, ε_0 is the vacuum permittivity, $\mathbf{d}$ is the dipole moment, $\mathbf{u}_{\mathbf{k}}(\mathbf{r}_0)$ are the eigenmodes of the Weyl system, and $\mathbf{r}_0$ is the atom location (see Sec. II in Ref. [32]). The SE rate Γ_{Weyl} is related to the emitted power P by $\Gamma_{\mathrm{Weyl}} = P/\hbar\omega_0$. Equation (2) reflects the modification of SE due to the optical environment in the steady-state limit, which corresponds to the Weisskopf-Wigner approximation in the quantum theory of the SE of a two-level atom in an inhomogeneous medium [34,41]. It is convenient to characterize the SE rate of the Weyl system Γ_{Weyl} by a dimensionless quantity, the Purcell factor $\mathrm{P}_{\mathrm{Weyl}}$, which is normalized by the rate of SE in free space Γ_0 as $\mathrm{P}_{\mathrm{Weyl}} = \Gamma_{\mathrm{Weyl}}/\Gamma_0$. According to Fermi's golden rule, the Purcell factor is proportional to the local photonic density of states in the surrounding Weyl system.

To quantitatively explore the SE of the Weyl medium across the transition between type I and type II, one needs to have the complete information of the eigenmode $\mathbf{u}_{\mathbf{k}}(\mathbf{r}_0)$ of the system, which entails the knowledge of the detailed design of the metamaterial. The realistic design of a photonic Weyl medium that can transit from type I to type II is based on the recent discovery of ideal Weyl degeneracies in a photonic metamaterial [27], in which all the Weyl points exist at the same energy and are well separated from any other bands. The ideal photonic Weyl metacrystal, being type I, possesses exact diminishing DOS and local DOS at the Weyl frequency. Figure 2(a) shows the structure of the ideal photonic Weyl metacrystal, which comprises of a saddle-shaped connective metallic coil that possesses D_{2d} point group symmetry in the tetragonal lattice. The unavoidable crossing between the longitudinal mode (LM) with negative dispersion and the transverse modes (TM) with positive dispersion in the metacrystal leads to the presence of type I Weyl points. The other three Weyl points are located on the $\Gamma - M$ at the same frequency with respect to $k_z = 0$ [Fig. 2(b)].

Interestingly, by rotating the metallic coil inside the cubic unit cell of the ideal photonic Weyl metacrystal about the z axis [Fig. 2(a)], we observe a continuous transition of the dispersion of LM of the Weyl metacrystal from negative to positive, as shown in Fig. 2(c), which indicates a transition from a type I Weyl system to a type II Weyl system. This transition arises from the variation of the spatial nonlocal effect. The location of the Weyl point also rotates with the rotation of the structure, which forms an angle θ with the $\Gamma - M$ direction (wave vector along $k_x = k_y$). The dispersion of the Weyl metacrystal along the Weyl vector k_{Weyl} with different rotation angles of 0°, 45°, and 34° are shown in Figs. 2(d)–2(f). As shown in Fig. 2(d), without rotation, the two bands of TM and LM in the Weyl metacrystal have opposite dispersion along $\Gamma - M$; their crossing forms a type I Weyl point. Dispersion of the Weyl metacrystal with a rotation angle of 45° is shown in Fig. 2(e). In this case, both the dispersions of the TM and LM modes are positive at the Weyl point, indicating that the Weyl point is type II. The critical transition of the Weyl point corresponding to $\alpha_{\mathrm{Weyl}} = 1$ occurs at a rotation angle around 34.1°, which shows a flat dispersion for the LM as shown in Fig. 2(f).

The finite size of the unit cell imposes a boundary that sets a three dimensional bound to the isofrequency surface in the Weyl system. Because of the spatial variation of the eigenmodes of the structured Weyl medium, the SE rate of an atom in the Weyl metacrystal is proportional to the local DOS of Weyl metacrystal, which is position dependent. Here we analyze the average SE rate for the atom position varied over the whole unit cell of the Weyl metacrystal based on the numerically acquired spatial distribution of the eigenmodes. Transformation of the average SE rate in the ideal Weyl metacrystal is illustrated by Fig. 3. As shown by Fig. 3(a), for a type I Weyl metacrystal, the SE spectrum exhibits a dip reaching zero

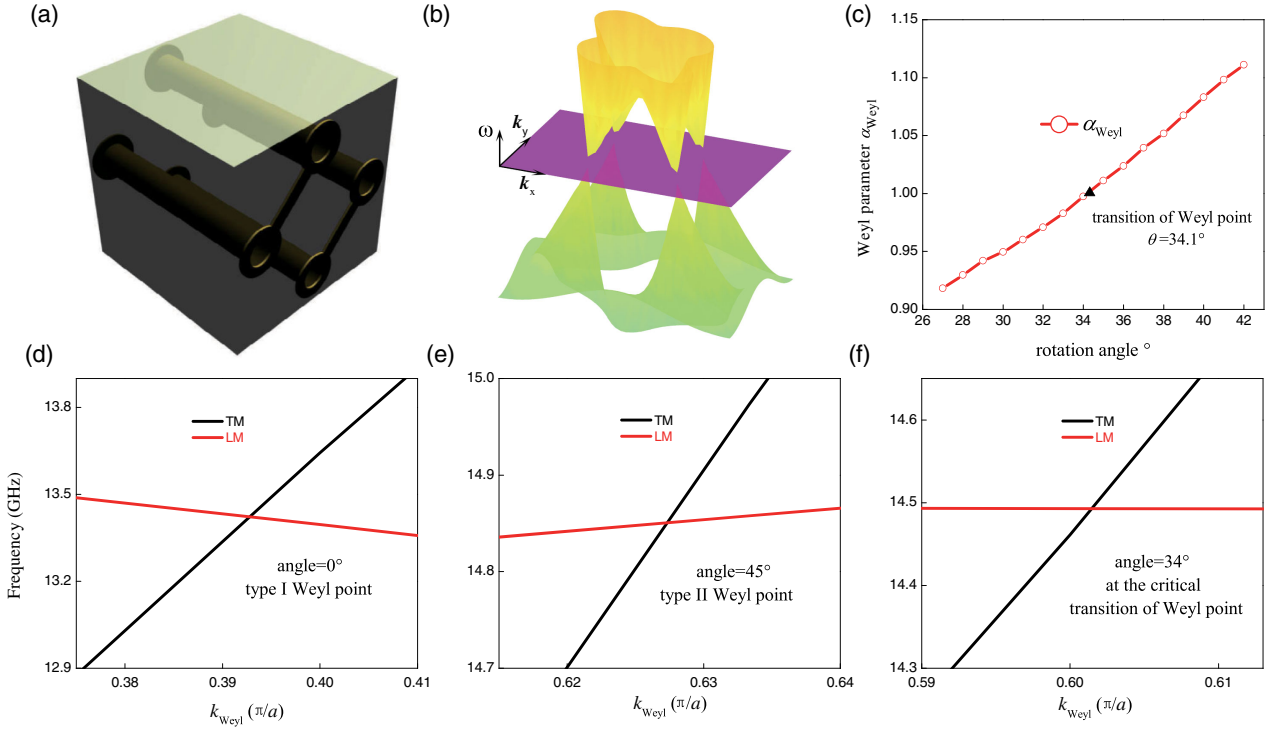

FIG. 2. (a) Schematic of a unit cell of saddle-shaped metallic inclusion, which has D_{2d} point group symmetry, embedded in a background medium with a dielectric constant of 2.2 at 10 GHz. The metallic coil rotates with an angle of 45° along the z direction. (b) Four type I Weyl points in the ideal photonic Weyl metacrystal reside on the same energy with respect of $k_z = 0$ (purple plane). (c) Variation of the Weyl parameter α_{Weyl} with rotation angle; the critical transition of the Weyl point from type I to type II occurs at a rotation angle of about 34.1°. (d)–(f) Dispersions of the Weyl metacrystal along the Weyl vector with different rotation angles 0°, 45°, and 34° representing the type I Weyl point, type II Weyl point, and the critical transition of the Weyl point, respectively.

at the Weyl frequency. When the rotation angle is increased towards the transition angle, the width of the valley is reduced, leading to an extremely sharp spectral feature [Fig. 3(c)]. When the rotation angle exceeds the transition angle ($\theta_{\mathrm{tran}} \approx 34.1°$), the Weyl metacrystal transits into type II, which leads to the vanishing of the valley and the formation of a resonant peak at the Weyl frequency [Fig. 3(b)]. The above observations are consistent with the analysis of the DOS based on the effective Hamiltonian shown in Fig. 1. The analysis demonstrates that the DOS of the Weyl system provides a good approximation for the general transformation of the averaged SE rate of a Weyl metacrystal.

Similar to SE, scattering of the electromagnetic wave by a resonant scatterer also critically depends on the isofrequency surface of the surrounding medium [42–44]. We consider a two-level system (TLS) of atoms embedded in the Weyl metacrystal. The TLS is initially in its ground state, the incident photon is an eigenmode of the Weyl medium, which is scattered by the TLS to all the eigenmodes

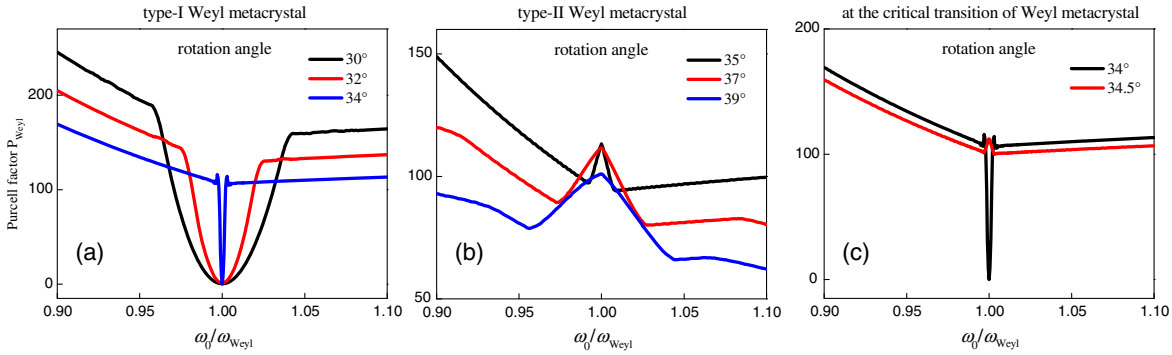

FIG. 3. Transformation of the SE rate of the ideal Weyl metacrystal. Rotation angle: (a) 30°–34° (type I), (b) 35°–39° (type II), respectively. (c) Transformation of the SE rate across the critical transition between the type I and type II Weyl system.

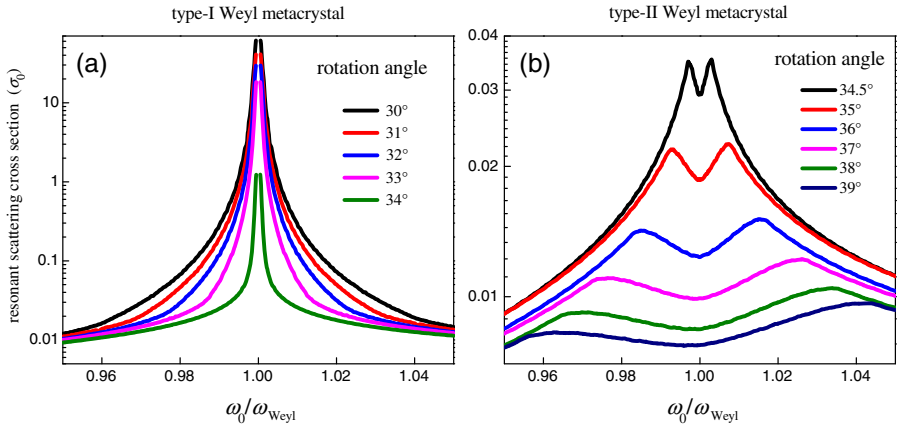

FIG. 4. Resonant scattering cross sections of type I (a) and type II (b) Weyl metacrystals, respectively. Rotation angle range: 30°–39°.

of the Weyl metacrystal. The scattering cross section of a resonant scatterer in the photonic Weyl structure is obtained by (see Sec. III in Ref. [32]):

$$\sigma(\mathbf{k},\omega_0)=\frac{1}{2\hbar\varepsilon_0}|\mathbf{d}\cdot\mathbf{u}_{\mathbf{k}}(\mathbf{r}_0)|^2\frac{\omega_{\mathbf{k}}}{|\mathbf{v}_{\mathbf{k}}|}\frac{\Gamma_{\mathrm{Weyl}}}{\Gamma_{\mathrm{Weyl}}^2/4+(\omega_{\mathbf{k}}-\omega_0)^2}. \tag{3}$$

The scattering cross section in the Weyl system averaged across the isofrequency surface can be obtained by integrating the cross section on the isofrequency surface, and divided by the area of the isofrequency surface [35–37]:

$$\bar{\sigma}(\omega_0)\propto\frac{1}{\iint d^2\mathbf{k}}\frac{\Gamma_{\mathrm{Weyl}}^2/4}{\Gamma_{\mathrm{Weyl}}^2/4+(\omega_{\mathbf{k}}-\omega_0)^2}, \tag{4}$$

where $\iint d^2\mathbf{k}=S_{\mathrm{Weyl}}$ is the area of isofrequency surface of the Weyl medium. Equation (4) shows that the spectral dependence of scattering cross section in Weyl system is similar to the well-known Breit-Wigner formula [38]. It should be noted from Eq. (4) that when the transition frequency of the two-level atom is the same as the Weyl frequency $\omega_{\mathbf{k}}=\omega_0$, the average scattering cross section is independent of the dipole polarization and location in the metacrystal, but only related to the area of the isofrequency surface of Weyl system.

Figure 4 shows the transformation of RSC around the transition between type I (a) and type II (b) Weyl metacrystals, numerically calculated by full wave simulation. The scattering cross section is normalized by the average cross section in free space $\sigma_0=\lambda^2/\pi$. It shows for a type I Weyl system, when approaching the Weyl frequency, the resonant scattering cross section is enhanced and finally diverges at the Weyl frequency [Fig. 4(a)]. The spectrum of RSC of the type I Weyl system exhibits a typical Lorentz line shape with bandwidth characterized by the SE rate. The RSC is extremely enhanced around the Weyl frequency, which comes at the price of the suppressed cross section slightly away from the resonant frequency. The area of isofrequency surface of the type I Weyl system close to the critical transition can be asymptotically described as $S_{\mathrm{Weyl}}\approx 3.11\pi\tilde{\omega}^2/[NN_x(1-\alpha_{\mathrm{Weyl}}^2)^{3/2}]$, where we have assumed $N_y=N_z=N$ for simplicity (see Sec. I in Ref. [32]). The area of the isofrequency surface diverges at the critical transition of the Weyl point. The average resonant cross section is inversely proportional to the area of isofrequency surface of the Weyl system, which scales as $\bar{\sigma}(\omega_0)\propto 1/S_{\mathrm{Weyl}}\propto(1-\alpha_{\mathrm{Weyl}}^2)^{3/2}/\tilde{\omega}^2$. This expression explains the extremely narrow RSC spectrum close to the critical transition [green curve in Fig. 4(a)].

On the contrary, due to the enhanced area of isofrequency surface of the type II Weyl metacrystal, the spectrum of RSC exhibits a dip around the Weyl frequency, and reaches the minimum right at the Weyl frequency (see Sec. IV in Ref. [32]). Further away from the critical transition point in the type II regime, the dip on the RSC spectrum becomes more broadened and lower [Fig. 4(b)]. Thus our study shows that the RSC of a type I and type II Weyl system exhibits opposite scattering features around the Weyl frequency, while the conversion of scattering cross section from peak to dip can be simply realized by tuning the rotation of the metallic coil in the ideal Weyl metacrystal, which shows exceptional flexibility and potential applications in manipulating wave-matter interactions.

In this work, we have studied the behaviors of SE and RSC in photonic Weyl metamaterials across the transition between type I and type II. Both SE and RSC show opposite features in type I and type II Weyl systems, whereas close to the transition point very sharp spectral features are present. Our analysis shows that the topological transformation of isofrequency surface of Weyl system plays the major role in such sharp features. Our findings on efficient modification of SE and scattering cross section in Weyl system provide rich potential applications in the photodetector with single frequency, high efficiency Weyl laser with tunable resonant frequency, etc.

The work is partially supported by an ERC Consolidator Grant (TOPOLOGICAL), the Royal Society and the Wolfson Foundation, the Leverhulme Trust (RPG-2012-674), and Horizon 2020 Action, Projects No. 734578 (D-SPA) and No. 777714 (NOCTORNO). Y. X. acknowledges support from the National Natural Science Foundation of China (Grant No. 11874269), the Guangdong Natural Science Foundation (Grant No. 2018A030313198), and the China Postdoctoral Science Foundation (Grant No. 2017M622746).

*These authors contribute equally to this work.
†Corresponding author.
yjxiang@szu.edu.cn
‡Corresponding author.
S.Zhang@bham.ac.uk

[1] E. M. Purcell, Spontaneous emission probabilities at radio frequencies, Phys. Rev. **69**, 681 (1946).
[2] S. Noda, M. Fujita, and T. Asano, Spontaneous emission control by photonic crystals and nanocavities, Nat. Photonics **1**, 449 (2007).
[3] P. Lodahl, A. F. vanDriel, I. S. Nikolaev, A. Irman, K. Overgaag, D. Vanmaekelbergh, and W. L. Vos, Controlling the dynamics of spontaneous emission from quantum dots by photonic crystals, Nature (London) **430**, 654 (2004).
[4] D. Englund, D. Fattal, E. Waks, G. Solomon, B. Zhang, T. Nakaoka, Y. Arakawa, Y. Yamamoto, and J. Vučković, Controlling the Spontaneous Emission Rate of Single Quantum Dots in a Two-Dimensional Photonic Crystal, Phys. Rev. Lett. **95**, 013904 (2005).
[5] P. Matthew, Modified spontaneous emission in nanophotonic structures, Nat. Photonics **9**, 427 (2015).
[6] S. Y. Zhu, Y. Yang, H. Chen, H. Zheng, and M. S. Zubairy, Spontaneous Radiation and Lamb Shift in Three-Dimensional Photonic Crystals, Phys. Rev. Lett. **84**, 2136 (2000).
[7] J. P. Reithmaier, G. Sęk, A. Löffler, C. Hofmann, S. Kuhn, S. Reitzenstein, L. V. Keldysh, V. D. Kulakovskii, T. L. Reinecke, and A. Forchel, Strong coupling in a single quantum dot semiconductor microcavity system, Nature (London) **432**, 197 (2004).
[8] X. Yang, J. Yao, J. Rho, X. Yin, and X. Zhang, Experimental realization of three dimensional indefinite cavities at the nanoscale with anomalous scaling laws, Nat. Photonics **6**, 450 (2012).
[9] C. Sauvan, J. P. Hugonin, I. S. Maksymov, and P. Lalanne, Theory of the Spontaneous Optical Emission of Nanosize Photonic and Plasmon Resonators, Phys. Rev. Lett. **110**, 237401 (2013).
[10] G. M. Akselrod, C. Argyropoulos, T. B. Hoang, C. Ciracì, C. Fang, J. Huang, D. R. Smith, and M. H. Mikkelsen, Probing the mechanisms of large Purcell enhancement in plasmonicnanoantennas, Nat. Photonics **8**, 835 (2014).
[11] D. Lu, J. J. Kan, E. E. Fullerton, and Z. Liu Enhancing spontaneous emission rates of molecules using nanopatterned multilayer hyperbolic metamaterials, Nat. Nanotechnol. **9**, 48 (2014).
[12] D. J. Roth *et al.*, Spontaneous emission inside a hyperbolic metamaterial waveguide, ACS Photonics **4**, 2513 (2017).
[13] F. D. M. Haldane and S. Raghu, Possible Realization of Directional Optical Waveguides in Photonic Crystals with Broken Time-Reversal Symmetry, Phys. Rev. Lett. **100**, 013904 (2008).
[14] Y. Poo, R. X. Wu, Z. Lin, Y. Yang, and C. T. Chan, Experimental Realization of Self-Guiding Unidirectional Electromagnetic Edge States, Phys. Rev. Lett. **106**, 093903 (2011).
[15] Z. Wang, Y. Chong, J. D. Joannopoulos, and M. Soljačić, Observation of unidirectional backscattering-immune topological electromagnetic states, Nature (London) **461**, 772 (2009).
[16] M. Hafezi, S. Mittal, J. Fan, A. Migdall, and J. M. Taylor, Imaging topological edge states in silicon photonics, Nat. Photonics **7**, 1001 (2013).
[17] S. Mittal, J. Fan, S. Faez, A. Migdall, J. M. Taylor, and M. Hafezi, Topologically Robust Transport of Photons in a Synthetic Gauge Field, Phys. Rev. Lett. **113**, 087403 (2014).
[18] A. B. Khanikaev, S. H. Mousavi, W. K. Tse, M. Kargarian, A. H. MacDonald, and G. Shvets, Photonic topological insulators, Nat. Mater. **12**, 233 (2013).
[19] W. Gao, M. Lawrence, B. Yang, F. Liu, F. Fang, B. Béri, J. Li, and S. Zhang, Topological Photonic Phase in Chiral Hyperbolic Metamaterials, Phys. Rev. Lett. **114**, 037402 (2015).
[20] L. Lu, Z. Wang, D. Ye, L. Ran, L. Fu, J. D. Joannopoulos, and M. Soljačić, Experimental observation of Weyl points, Science **349**, 622 (2015).
[21] M. Xiao, W.-J. Chen, W.-Y. He, and C. T. Chan, Synthetic gauge flux and Weyl points in acoustic systems, Nat. Phys. **11**, 920 (2015).
[22] L. Lu, L. Fu, J. D. Joannopoulos, and M. Soljačić, Weyl points and line nodes in gyroid photonic crystals, Nat. Photonics **7**, 294 (2013).
[23] F. Li, X. Huang, J. Lu, J. Ma, and Z. Liu, Weyl points and Fermi arcs in a chiral phononic crystal, Nat. Phys. **14**, 30 (2018).
[24] Q. Wang, M. Xiao, H. Liu, S. Zhu, and C. T. Chan, Optical Interface States Protected by Synthetic Weyl Points, Phys. Rev. X **7**, 031032 (2017).
[25] M. Xiao, Q. Lin, and S. Fan, Hyperbolic Weyl Point in Reciprocal Chiral Metamaterials, Phys. Rev. Lett. **117**, 057401 (2016).
[26] A. Poddubny, I. Iorsh, P. Belov, and Y. Kivshar, Hyperbolic metamaterials, Nat. Photonics **7**, 948 (2013).
[27] B. Yang *et al.*, Ideal Weyl points and helicoid surface states in artificial photonic crystal structures, Science **359**, 1013 (2018).
[28] A. A. Soluyanov, D. Gresch, Z. Wang, Q. Wu, M. Troyer, X. Dai, and B. A. Bernevig, Type II Weyl semimetals, Nature (London) **527**, 495 (2015).
[29] L. Novotny and B. Hecht, *Principles of Nano-optics* (Cambridge University Press, Cambridge, England, 2006).
[30] W. Yan, M. Wubs, and N. A. Mortensen, Hyperbolic metamaterials: Nonlocal response regularizes broadband super singularity, Phys. Rev. B **86**, 205429 (2012).
[31] Y. P. Chen, W. E. I. Sha, W. C. H. Choy, L. J. Jiang, and W. C. Chew, Study on spontaneous emission incomplex

multilayered plasmonic system via surface integral equation approach with layered medium Green's function, Opt. Express **20**, 20210 (2012).

[32] See Supplemental Material at http://link.aps.org/supplemental/10.1103/PhysRevLett.123.033901 for discussions about the analytical derivation of density of states and the area of isofrequency surface of the type I system, scattering in the Weyl system, and transformation of the area of isofrequency surface in different types of Weyl metacrystals, which includes Refs. [6,33–38].

[33] D. N. Chigrin, Radiation pattern of a classical dipole in a photonic crystal: Photon focusing, Phys. Rev. E **70**, 056611 (2004).

[34] V. Weisskopf and E. Wigner, Berechnung der natürlichen Linienbreite auf Grund der Diracschen Lichttheorie, Z. Phys. **63**, 54 (1930).

[35] J. Liu, M. Zhou, and Z. Yu, Quantum scattering theory of a single-photon Fock state in three dimensional spaces, Opt. Lett. **41**, 4166 (2016).

[36] M. Zhou, L. Ying, L. Lu, L. Shi, J. Zi, and Z. F. Yu, Electromagnetic scattering laws in Weyl systems, Nat. Commun. **8**, 1388 (2017).

[37] X. H. Wang, Y. S. Kivshar, and B. Y. Gu, Giant Lamb Shift in Photonic Crystals, Phys. Rev. Lett. **93**, 073901 (2004).

[38] J. J. Sakurai and J. Napolitano, *Modern Quantum Mechanics* (Addison-Wesley, Reading, MA, 2011).

[39] J. P. Dowling and C. M. Bowden, Atomic emission rates in inhomogeneous media with applications to photonic band structures, Phys. Rev. A **46**, 612 (1992).

[40] Z. Y. Li, L. L. Lin, and Z. Q. Zhang, Spontaneous Emission from Photonic Crystals: Full Vectorial Calculations, Phys. Rev. Lett. **84**, 4341 (2000).

[41] K. Busch, N. Vats, S. John, and B. C. Sanders, Radiating dipoles in photonic crystals, Phys. Rev. E **62**, 4251 (2000).

[42] J. T. Shen and S. Fan, Strongly Correlated Two-Photon Transport in a One-Dimensional Waveguide Coupled to a Two-Level System, Phys. Rev. Lett. **98**, 153003 (2007).

[43] E. Shahmoon, D. S. Wild, M. D. Lukin, and S. F. Yelin Cooperative Resonances in Light Scattering From Two-Dimensional Atomic Arrays, Phys. Rev. Lett. **118**, 113601 (2017).

[44] H. N. S. Krishnamoorthy, Z. Jacob, E. Narimanov, I. Kretzschmar, and V. M. Menon, Topological transitions in metamaterials, Science **336**, 205 (2012).